JACS
JOURNAL OF THE AMERICAN CHEMICAL SOCIETY

Article

pubs.acs.org/JACS

Azulene Methacrylate Polymers: Synthesis, Electronic Properties, and Solar Cell Fabrication

Egle Puodziukynaite,[†] Hsin-Wei Wang,[†] Jimmy Lawrence,[†] Adam J. Wise,[‡] Thomas P. Russell,[†] Michael D. Barnes,[‡] and Todd Emrick*[,†]

[†]Polymer Science and Engineering Department and [‡]Department of Chemistry, University of Massachusetts Amherst, 120 Governors Drive, Amherst, Massachusetts 01003, United States

Supporting Information

ABSTRACT: We report the synthesis of novel azulene-substituted methacrylate polymers by free radical polymerization, in which the azulene moieties represent hydrophobic dipoles strung pendant to the polymer backbone and impart unique electronic properties to the polymers. Tunable optoelectronic properties were realized by adjusting the azulene density, ranging from homopolymers (having one azulene group per repeat unit) to copolymers in which the azulene density was diluted with other pendant groups. Treating these polymers with organic acids revealed optical and excitonic behavior that depended critically on the azulene density along the polymer chain. Copolymers of azulene with zwitterionic methacrylates proved useful as cathode modification layers in bulk-heterojunction solar cells, where the relative azulene content affected the device metrics and the power conversion efficiency reached 7.9%.

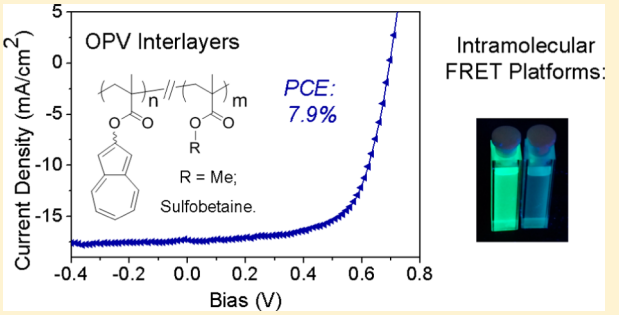

1. INTRODUCTION

Developments in organic electronics are enabled by novel materials, architectures, and interfacial engineering[1,2] and benefit from multicomponent polymers that integrate electronically active structures into otherwise insulating backbones. Azulene, a vibrant-blue 10-π-electron isomer of naphthalene, gains stabilization from resonance contributions of cyclopentadienyl anion and tropylium cation; this "donor−acceptor" resonance structure affords a dipole moment (>1 D) that distinguishes azulene from conventional fused benzenoids.[3−6] The optoelectronic characteristics of azulene can be manipulated by (reversible) protonation with strong acids, altering its absorption profile and leading to S_1 excited state emission.[7−10] Because of their unique optical and electronic properties, azulene-based structures are useful in charge-transport,[11,12] nonlinear optics,[13,14] and sensor applications.[15] The combination of their dipolar nature, high polarizability, and ion/metal complexation capability[16,17] renders azulene derivatives attractive candidates for functional composite architectures and self-assembled structures. However, the relative lack of azulene-containing polymer materials limits their availability in numerous materials applications.

To date, the preparation of azulene-based polymers has centered on conjugated structures with azulene as the repeat unit, in which the polymer backbone extends through the five- or seven-membered ring, as seen for example in the reports of Hawker[8] and Lai.[12] To our knowledge, reports on chain-growth polymers with pendant azulene groups are lacking, despite the potential utility of such structures as processable materials with well-defined azulene density. Okawara and co-workers reported an attempted polymerization of azulene-substituted acrylates, in which azulene was thought to be responsible for inhibiting homopolymerization and retarding copolymerization with styrene.[18] Our polymerization of azulene-substituted methacrylates hinged on a new monomer design and thus did not suffer from such complications, providing straightforward access to both homopolymers and copolymers with tunable azulene density along the backbone. Adjusting the azulene density with interspersed polar or apolar comonomers dictated the photophysical properties, electronic interactions, and exciton migration between pendant units. While the azulene-based polymers we describe may have numerous applications in electronic materials, we chose to examine their role as interlayers in bulk-heterojunction solar cells, specifically as cathode modification layers intended to improve device efficiency.

2. RESULTS AND DISCUSSION

2.1. Synthesis. Azulene-based methacrylate homopolymers as well as copolymers with methyl methacrylate and sulfobetaine methacrylate were synthesized from the novel azulene methacrylates as shown in Figures 1 and 2. 2-Hydroxyazulene (**4**), the common starting material for monomers **5** and **10**, was synthesized by condensation of 2-chlorotropone (**2**) with diethyl acetone-1,3-dicarboxylate

Received: May 13, 2014

   dx.doi.org/10.1021/ja504670k | J. Am. Chem. Soc. XXXX, XXX, XXX−XXX

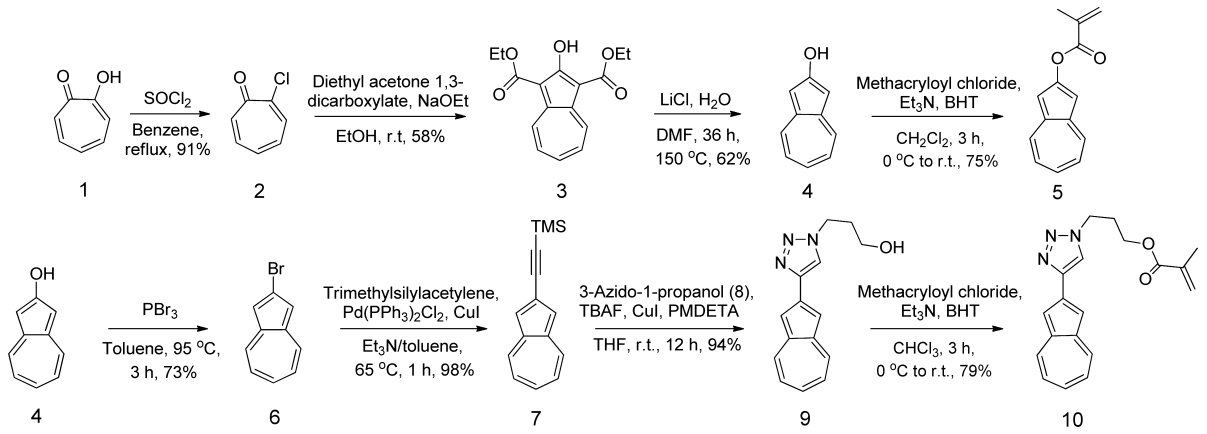

Figure 1. Preparation of azulene methacrylates **5** and **10**.

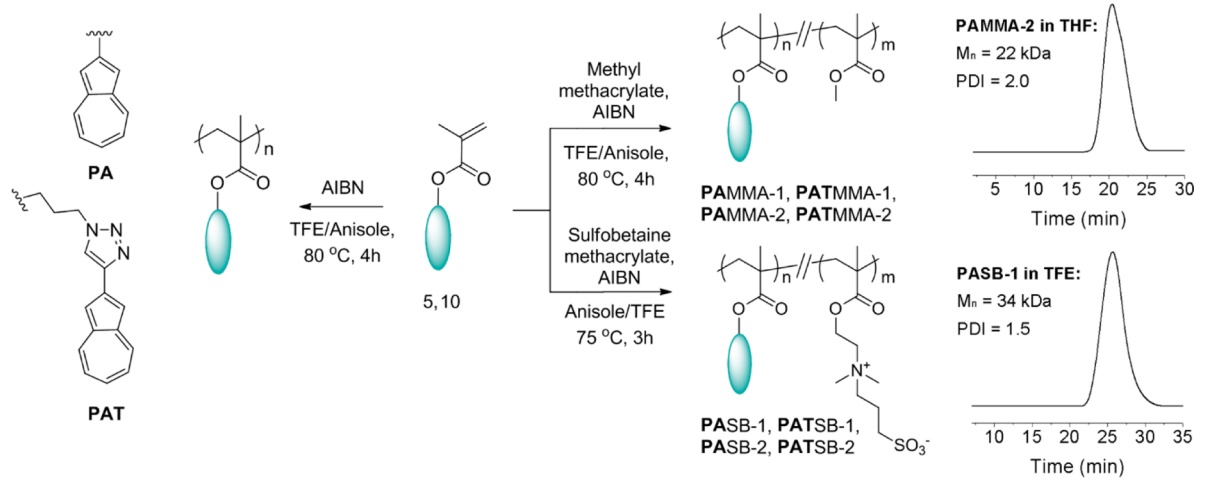

Figure 2. Homo- and copolymerization of azulene methacrylates **5** and **10** and representative gel-permeation chromatography (GPC) traces (far right).

followed by decarboxylation.[9] Azulen-2-yl methacrylate (**5**) was isolated as a deep-purple solid in 75% yield by the reaction of **4** with methacryloyl chloride in the presence of triethylamine and butylated hydroxytoluene (BHT) as a free radical scavenger. 2-Bromoazulene (**6**), our chosen precursor to monomer **10**, was obtained in 73% yield by the reaction of **4** with PBr_3. Sonogashira coupling of **6** with trimethylsilylacetylene gave **7**,[9] and subsequent in situ TMS deprotection and copper-catalyzed azide−alkyne cycloaddition with 3-azido-1-propanol (note safety comment in Supporting Information) afforded triazole **9**. The reaction of **9** with methacryloyl chloride gave monomer **10** as a blue solid. Each monomer synthesis proved to be easily scalable to gram quantities.

Azulene methacrylates **5** and **10** were amenable to free radical polymerization using azobis(isobutyronitrile) (AIBN) initiation, affording the respective polymers in 73 and 82% yield (Figure 2 and Table 1). These azulene (**PA**) and azulene-triazole (**PAT**) methacrylate homopolymers with molecular weight (MW) values of <15 kDa had sufficient solubility for solution characterization. Copolymerization of azulenes **5** and **10** with methyl methacrylate (MMA) gave polymers with a tunable average interchromophore distance and good solubility in organic solvents for characterization. **PAMMA** and **PATMMA** copolymers containing 20−40 mol % azulene were obtained with number-average molecular weight (M_n) values ranging from 14 to 22 kDa and polydispersity indices (PDIs) of 1.7−2.6. Copolymerization of the azulene monomers with sulfobetaine (SB) methacrylate afforded polymers with M_n values of 19−39 kDa and PDIs of 1.5−1.7. While incorporation of monomer **5** into the SB-based copolymers was limited by the solubility of the resulting polymers, **PATSB** copolymers with high azulene content (>70 mol %) retained favorable solubility, leading to their facile implementation into devices (described

Table 1. GPC-Estimated M_n and PDI Values of Azulene-Containing Polymers with Variable Mole Percentages of 5 and 10

	azulene (mol %)			
polymer	feed	incorporated[a]	M_n (kDa)	PDI
PA	100	100	13.5	2.5
PAMMA-1	14	22	17.2	1.8
PAMMA-2	25	40	22.0	2.0
PASB-1	25	25	33.5	1.5
PASB-2	50	45	18.9	1.6
PAT	100	100	13.6	2.2
PATMMA-1	14	19	20.5	1.7
PATMMA-2	25	36	13.9	2.6
PATSB-1	25	24	38.9	1.7
PATSB-2	50	49	28.4	1.7
PATSB-3	75	76	25.4	1.7

[a]As determined by ^{1}H NMR spectroscopy.

dx.doi.org/10.1021/ja504670k | J. Am. Chem. Soc. XXXX, XXX, XXX−XXX

later). All of the polymers in the **PA** and **PAT** series were obtained as purple or blue solids, respectively. For **PA**, the protons of the pendant azulene units were identified as broad ^{1}H NMR ($CDCl_3$) signals at 7.88 (4- and 8-positions), 7.49 (6-position), and 7.06 ppm (1-, 3-, 5-, and 7-positions). For **PAT**, the azulene proton signals appeared at 8.01 (4- and 8-positions), 7.51 (1- and 3-positions), 7.36 (6-position), and 6.97 ppm (5 and 7-positions), whereas the proton resonance of the triazole ring appeared at 7.85 ppm. Polymerizations were conducted in anisole, freshly distilled 2,2,2-trifluoroethanol (TFE), or mixtures of the two, and maintaining solubility during the polymerization was crucial to achieving high monomer conversion. In addition, two azulene acetates, **A-M** and **AT-M** (Figure 3), were prepared as model systems [Scheme S1; detailed syntheses are provided in the Supporting Information (SI)].

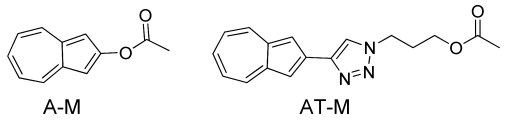

Figure 3. Azulene model compounds **A-M** and **AT-M**.

Azulene exhibits a ground-state dipole moment (μ) of 1.08 D.[3] To determine the impact of substituents, the model compounds **A-M** and **AT-M** were examined by density functional theory calculations at the B3LYP/6-311G+(d,p)//B3LYP/6-311G+(d,p) level [μ_{calc}(azulene) = 1.08 D]. **A-M** and **AT-M** were calculated to possess larger dipole moments than azulene itself (5.8 and 4.0 D, respectively), suggesting a substantive effect of these substituents on the electronic properties of azulene resulting from extension of the structure through the 2-position (along the dipole).[11,19] The calculated molecular orbital (MO) distributions for **A-M** and **AT-M** further indicate a direct effect of 2-substitution on the lowest unoccupied MO (LUMO) level (Figure S1 in the SI).[4,5,20]

2.2. Optical Properties. The photophysical features reported for azulene (Az) and azulinium cation [Az + H^+] are unique among fused aromatic hydrocarbons[21,22] and useful for comparison to the polymer structures and model compounds we have prepared. Figure 4 shows solution absorption spectra of azulene, **A-M**, and **AT-M**. The visible absorption (~575 nm) corresponds to an S_0 ($^1A_1$) → S_1 ($^1B_1$) electronic transition, while the much stronger absorption near

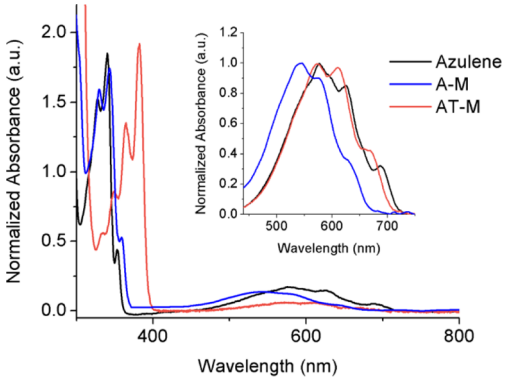

Figure 4. Normalized solution absorption spectra of azulene, **A-M**, and **AT-M** in chloroform. The inset shows the weak S_0 ($^1A_1$) → S_1 ($^1B_1$) absorption normalized for clarity.

350 nm corresponds to an S_0 ($^1A_1$) → S_2 ($^1A_1$) transition.[21] These visible and UV absorptions represent transitions polarized perpendicular and parallel to the C_2 axis, respectively, and the very small oscillator strength of the S_0 ($^1A_1$) → S_1 ($^1B_1$) transition[21] is due to small differences in the electron densities of the two states (particularly between C9 and C10). Thus, excitation with visible wavelengths lead to primarily non-radiative decay,[23,24] and only weak photoluminescence (PL) originating from the S_2 state (in violation of Kasha's rule[25]) is observed for neutral azulenes (Figure S2 in the SI).[26,27]

Treatment with acid (such as trifluoroacetic acid, TFA) protonates azulene at C1 or C3, forming [Az + H^+] and generating a new absorption with a transition energy intermediate between those of the Az S_0 → S_1 and S_0 → S_2 bands, appearing at 355 nm (Figure S3 in the SI).[28,29] Figure 5

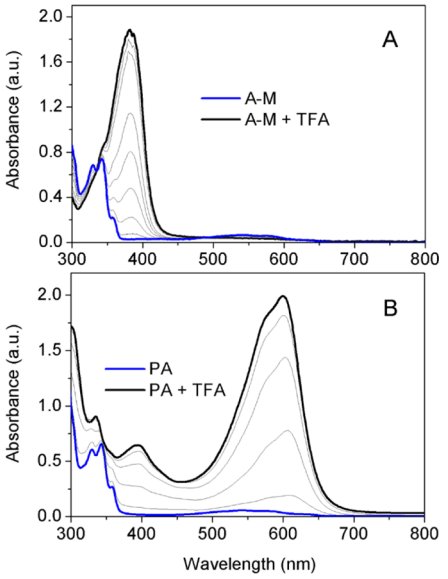

Figure 5. UV−vis absorption spectra of dilute chloroform solutions of (A) **A-M** and (B) **PA** upon addition of TFA. Gray lines indicate the evolution (growth) of the absorption intensity with continuous addition of TFA.

shows absorption spectra of **A-M**, **PA**, before and after treatment with TFA. For **A-M**, the absorption associated with [Az + H^+] dominates the spectrum at high TFA concentration. For **PA**, the same [Az + H^+] absorption (slightly red-shifted) is observed as well as a new strong absorption near 600 nm. This feature is also seen for **PAMMA-1** and **PAMMA-2** solutions as well as thin **A-M** films treated with TFA vapor (Figures S4 and S5 in the SI). Such differences between the solution absorption spectra of the model compound and the polymers may arise from complexation with TFA, σ-dimer formation, or a Stark effect.[12,30−32] The latter hypothesis is supported by the close proximity of this absorption to the neutral Az S_0 → S_1 band (and the associated 0.13 eV red-shift), suggesting a perturbation of the Az absorption signature. In the **PA** polymer, a neutral Az moiety situated near (<1 nm) a protonated pendant Az group may experience a strong Stark effect from the direct-current (DC) field generated by the localized proton. The resultant mixing of the $^1B_1$ excited state with states of different (b-type) symmetry, depending on the precise orientation of the two adjacent Az moieties, would enhance the S_0 → S_1 transition moment for the neutral Az,

dx.doi.org/10.1021/ja504670k | J. Am. Chem. Soc. XXXX, XXX, XXX−XXX

giving rise to the strong absorption in the visible spectral region.

We were intrigued to note that the spectral properties of **AT-M** and **PAT** evolve differently with addition of TFA. Figure 6

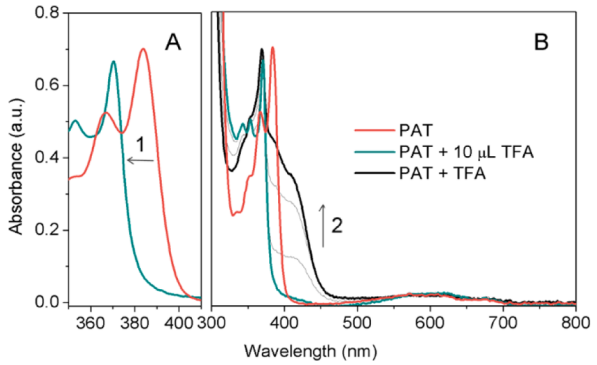

Figure 6. UV−vis absorption spectra of a dilute chloroform solution of **PAT** upon addition of TFA, demonstrating sequential protonation of the triazole (red curves to cyan curves in A and B) and azulene (cyan curve to black curve in B) moieties. Gray lines in (B) indicate the growth in absorption intensity with addition of TFA. "1" denotes the shift due to triazole protonation, and "2" denotes changes in absorption intensity with azulene doping.

and Figure S6 in the SI show representative absorption spectra of **PAT** and **AT-M**, respectively, with increasing TFA concentration. Two distinct spectral features were observed: (1) a rapid blue shift in the near-UV absorption, attributed to protonation of the triazole ring and an alteration of the aromaticity in the triazole, and (2) a slower growth in the azulene absorption intensity near 400 nm. The red shift of the azulinium absorption of **PAT** relative to those of **A-M** and **PA** is attributed to the increased conjugation length. The absence of the strong absorption at 600 nm in the protonated **PAT** system is noteworthy and can be rationalized by considering the weaker electronic interactions between the charged (protonated) triazole and neighboring azulenes due to their larger separation distance.

Photoluminescence quenching was used to probe the electronic interactions between protonated and neutral pendant azulene moieties in the **PA** and **PAT** polymer families. Because of the low oscillator strength of the $S_0 \rightarrow S_1$ transition in neutral azulene, the neutral system is essentially nonfluorescent (i.e., nonradiative decay dominates). On the other hand, visible PL from the azulinium cation is readily observed. Figure 7A shows PL spectra of azulene, **A-M**, and **AT-M** upon addition of TFA, excited near the azulinium absorption maximum. Small shifts in the peak PL wavelength for the different species were observed: both the **A-M** and **AT-M** PL spectra were red-shifted with respect to that of (pure) azulinium, while the peak of **AT-M** was red-shifted by 50 nm (250 meV) with respect to **A-M**, consistent with the extended conjugation length of protonated **AT-M**.

Time-resolved photoluminescence of the azulene monomers and polymers shows evidence of polymer-specific chromophore interactions. Figure 8A shows PL decay profiles obtained from **A-M**, **PA**, and **PAMMA-2** upon addition of TFA and excited in the azulinium band at 405 nm (20 ps pulse width; 40 MHz repetition rate). The protonated molecules show similar single-exponential decays with time constants of ∼2.2 ns. Figure 8B shows the PL decay profiles of **AT-M**, **PAT**, and **PATMMA-1**.

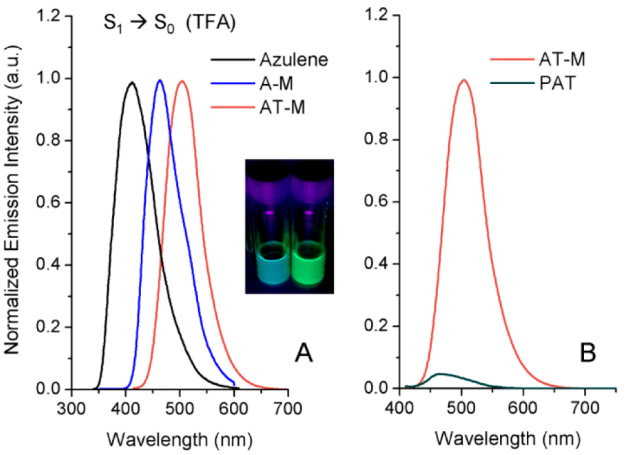

Figure 7. (A) Normalized emission spectra of azulene, **A-M**, and **AT-M** in their protonated states ($S_1 \rightarrow S_0$) as dilute chloroform solutions. (B) Normalized PL spectra of **AT-M** and **PAT** ($S_1 \rightarrow S_0$) as dilute chloroform solutions with equal absorption intensities at the excitation wavelength, indicating that the azulinium luminescence is significantly quenched in the **PAT** system.

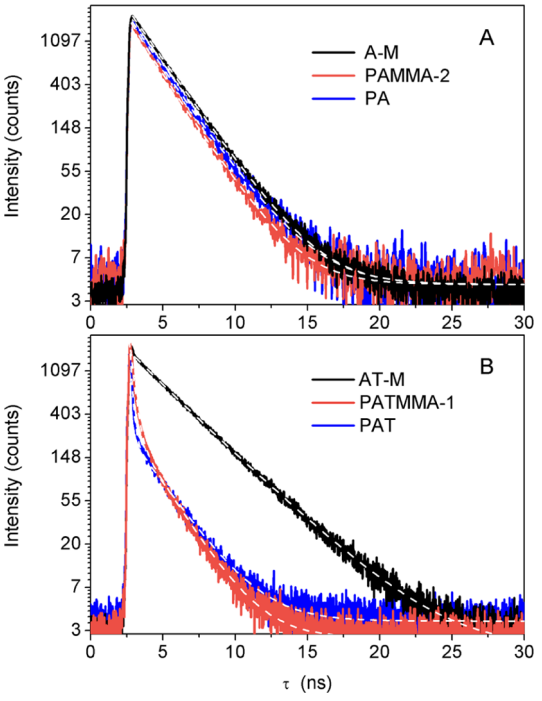

Figure 8. Time-resolved PL spectra and the respective exponential fits of (A) **A-M**, **PA**, and **PAMMA-2** and (B) **AT-M**, **PAT**, and **PATMMA-1** in dilute chloroform solutions upon the addition of TFA.

Interestingly, while the PL decay of the **PA** family is characterized by a *single-exponential decay* of azulinium, the **PAT** family shows *biexponential decay* with a fast-decay time constant of 150 ps for **PAT** and 260 ps for **PATMMA-1** (Table S1 in the SI). The slow-decay time constant (∼2 ns) was identified as that for the normal azulinium cation decay. Comparison of the PL spectra of **AT-M** and **PAT** under conditions of roughly equal absorbance shows that the PL in protonated **PAT** is strongly quenched (Figure 7B), and thus, the fast PL decay in the time-resolved measurements reflects the quenching rate rather than a new radiative process.

dx.doi.org/10.1021/ja504670k | J. Am. Chem. Soc. XXXX, XXX, XXX−XXX

A plausible mechanism for the PL quenching observed for the **PAT** family is energy transfer from protonated pendant azulene triazole moieties to neighboring neutral (or singly protonated) species. Figure 9 shows the scaled azulinium

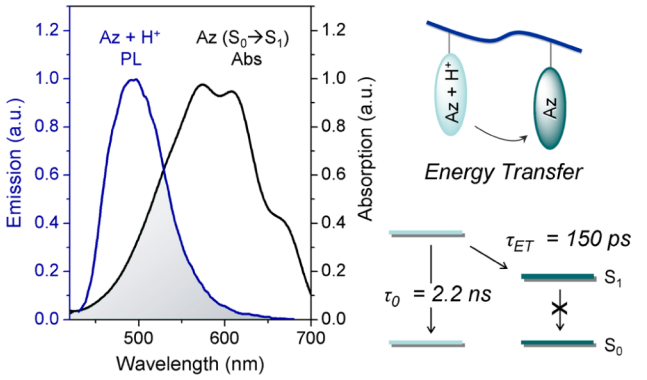

Figure 9. (Left) Emission (blue) and $S_0 \rightarrow S_1$ absorption (black) spectra of triazole azulinium and neutral azulene species (for **AT-M**). The integrated area between the two (shaded) defines the Förster radius for energy transfer (R_0). (Right) Schematic illustration of energy transfer from triazole azulinium to neutral azulene with associated time constants (for **PAT**).

(donor) PL spectrum and the unperturbed $S_0 \rightarrow S_1$ absorption for neutral azulene of **AT-M**. We computed a Förster radius of 1.5 nm for energy transfer between neighboring azulinium and azulene moieties (see the SI). From the relation $\tau \approx \tau_0 (r/R_0)^6$, where R_0 is the Förster radius, r is the interchromophore separation, and τ_0 is the azulinium natural radiative lifetime, we compute a quenching lifetime (inverse rate) of 190 ps at an r value of 1 nm. Thus, the observed fast-decay component (150 ps) in the **PAT** photoluminescence is consistent with an energy transfer mechanism. To explain why energy transfer occurs in **PAT** and not **PA**, we suggest that the 130 meV red shift observed for the $S_0 \rightarrow S_1$ transition (possibly a Stark perturbation) in the protonated **PA** system reduces the Förster radius and effectively turns off the energy transfer decay pathway. Moreover, we speculate that the probability of finding an energy transfer partner (i.e., a neutral azulene) is greater in the **PAT** family because of the presence of the triazole moiety. We note that such unique aspects found for these azulene-based polymers are not observed for naphthalene-based systems, which exhibit $S_1 \rightarrow S_0$ emission, excimer formation, and no fluorescence switching in the presence of acid.[5,33,34]

2.3. Solar Cells. We examined whether the integration of azulene into polymers would have any ramifications for conducting materials and/or devices. Polyelectrolytes and polymer zwitterions can modify the work function (WF) of metals, affording composite electrodes that represent a route to improved power conversion efficiency (PCE) in solar cells.[1,2,35,36] Polymer zwitterions represent particularly attractive platforms because of their orthogonal solubility with active-layer polymers and the absence of counterions that can degrade device performance. **PA**- and **PAT**-based copolymers with sulfobetaine methacrylate having two types of dipoles, one hydrophobic (azulene) and one hydrophilic (SB), were thus examined in devices having an active layer of PTB7 and $PC_{71}BM$, with Ag chosen as the cathode for its excellent stability and amenability to WF modification. In a typical solar cell architecture, thin (≤5 nm) zwitterionic azulene methacrylate copolymer interlayers were deposited by spin-coating onto the PTB7:$PC_{71}BM$ active layer, which was prepared on an ITO/PEDOT:PSS anode, followed by thermal evaporation of a Ag cathode. Control devices featuring poly(sulfobetaine methacrylate) (**PSBMA**) interlayers as well as those containing bare silver electrodes were also constructed and characterized. Key characteristics of the fabricated solar cells are summarized in Figures 10 and 11.

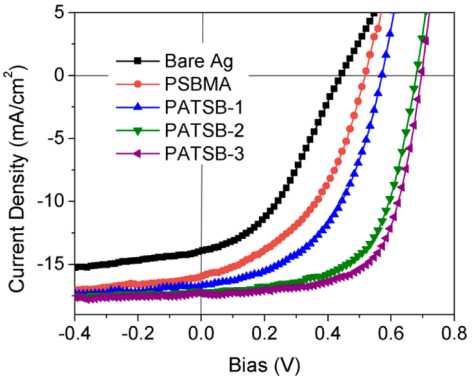

Figure 10. *J*–*V* characteristics of solar cells with a bare Ag cathode and with polymers interlayers containing azulene and sulfobetaine.

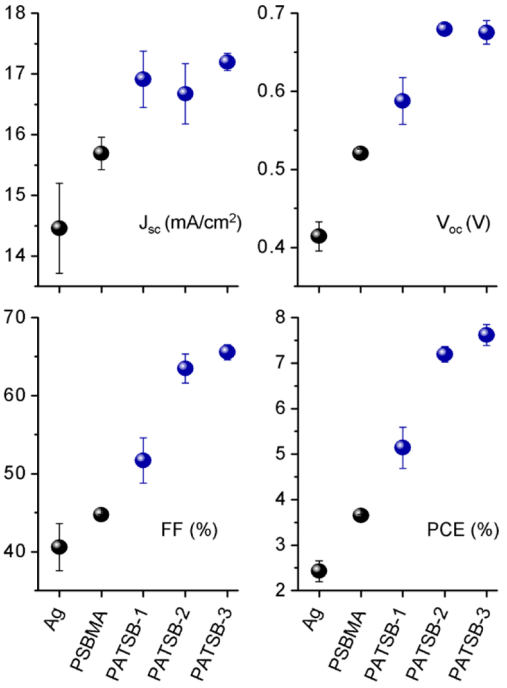

Figure 11. Characteristics of solar cells with a bare Ag cathode and with cathode modification layers containing azulene and sulfobetaine.

Device performance generally increased with azulene density in the interlayer polymers. The average PCE values for bare Ag, **PSBMA**, **PATSB-1**, and **PATSB-2** were 2.4%, 3.7%, 5.1%, and 7.2%, respectively. Notably, the **PATSB-3** copolymers, having highest azulene content (~75 mol % azulene), gave the highest efficiencies: the average PCE was 7.6%, and the best-performing device reached a PCE of 7.9%. **PASB-1** and **PASB-2** polymers were also found to be effective as interlayers, enabling organic photovoltaic (OPV) device efficiencies of 6.0% and 7.1%, respectively (Table S2, Figure S7, SI). As shown in Figure 11, the increase in efficiency was mainly due to a higher open-

dx.doi.org/10.1021/ja504670k | J. Am. Chem. Soc. XXXX, XXX, XXX–XXX

circuit voltage (V_{oc}), with smaller contributions from the short-circuit current density (J_{sc}) and the fill factor (FF). It is noteworthy that azulene-functionalized sulfobetaine methacrylates, when used as interlayers, were found to exhibit comparable or superior performance to the respective conjugated-polymer-based structures.[36,37] Additionally, devices fabricated with these interlayers outperformed the commonly used LiF cathode modifier while offering the additional benefits of air stability and compatibility with solution and roll-to-roll processing.[36] V_{oc} enhancements in devices with cathode modifiers may arise from the respective WF reduction at the electrode, creating a built-in potential gradient across the active layer between the electrodes. In addition, such electrode modifications allow for increases in J_{sc} and FF via charge extraction control and recombination reduction. To gain additional insight into the performance mechanism of zwitterionic azulene-containing polymers, thin films of the respective polymers on Ag substrates were studied by ultraviolet photoelectron spectroscopy (UPS). UPS was used to measure the WF of the substrates, revealing an interfacial dipole as a result of the polymer coatings (Figure 12).

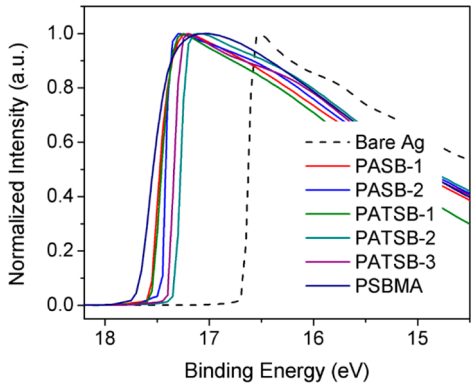

Figure 12. UPS results for bare Ag, **PSBMA**, and azulene-containing **PASB** and **PATSB** copolymers.

The absolute magnitude of the Δ values, derived from the difference between the secondary electron cutoff energies (E_{SEC}) of Ag and polymer-coated Ag, were in the range of 0.66−1.07 eV for the zwitterionic homo- and copolymers. That the azulene-based methacrylate interlayers outperformed the pure sulfobetaine zwitterion polymer in devices (i.e., **PSBMA**, which gave the largest Δ value) provides compelling evidence for the importance of factors beyond the interfacial dipole, such as surface wetting. Atomic force microscopy (AFM) measurements revealed **PSBMA** to provide nonuniform coverage of the active layer, whereas the azulene-based polyzwitterions afforded a smooth coverage as would be desired in an interlayer material (Figure S8 in the SI).

SUMMARY

A new functional polymer platform was realized through the preparation of azulene-substituted methacrylate monomers and their successful use in chain-growth polymerization. Controlling the density of pendant azulene groups along the polymer backbone dictated the optical properties and excitonic interactions upon acid doping, distinguishing this polymer platform from simple substituted azulenes. Azulene copolymers with sulfobetaine methacrylate were found to be remarkably effective as cathode modification layers in OPV devices, giving PCE values approaching 8%.

ASSOCIATED CONTENT

Supporting Information

Experimental procedures and additional synthesis, photophysical, and device characterization data. This material is available free of charge via the Internet at http://pubs.acs.org.

AUTHOR INFORMATION

Corresponding Author

tsemrick@mail.pse.umass.edu

Notes

The authors declare no competing financial interest.

ACKNOWLEDGMENTS

The authors acknowledge support from the National Science Foundation (NSF-CHE-1152360, T.E.) associated with polymer synthesis and the Department of Energy-supported Energy Frontier Research Center (EFRC) at UMass Amherst (H.W.W., T.P.R.) for solar cell fabrication and characterization.

REFERENCES

(1) Zhou, Y.; Fuentes-Hernandez, C.; Shim, J.; Meyer, J.; Giordano, A. J.; Li, H.; Winget, P.; Papadopoulos, T.; Cheun, H.; Kim, J.; Fenoll, M.; Dindar, A.; Haske, W.; Najafabadi, E.; Khan, T. M.; Sojoudi, H.; Barlow, S.; Graham, S.; Brédas, J.-L.; Marder, S. R.; Kahn, A.; Kippelen, B. *Science* **2012**, *336*, 327−332.
(2) He, Z.; Zhong, C.; Su, S.; Xu, M.; Wu, H.; Cao, Y. *Nat. Photonics* **2012**, *6*, 593−597.
(3) Anderson, A. G.; Steckler, B. M. *J. Am. Chem. Soc.* **1959**, *81*, 4941−4946.
(4) Lemal, D. M.; Goldman, G. D. *J. Chem. Educ.* **1988**, *65*, 923−925.
(5) Michl, J.; Thulstrup, E. W. *Tetrahedron* **1976**, *32*, 205−209.
(6) Robb, M. J.; Ku, S.-Y.; Brunetti, F. G.; Hawker, C. J. *J. Polym. Sci., Part A: Polym. Chem.* **2013**, *51*, 1263−1271.
(7) Amir, E.; Amir, R. J.; Campos, L. M.; Hawker, C. J. *J. Am. Chem. Soc.* **2011**, *133*, 10046−10049.
(8) Murai, M.; Amir, E.; Amir, R. J.; Hawker, C. J. *Chem. Sci.* **2012**, *3*, 2721−2725.
(9) Koch, M.; Blacque, O.; Venkatesan, K. *Org. Lett.* **2012**, *14*, 1580−1583.
(10) Koch, M.; Blacque, O.; Venkatesan, K. *J. Mater. Chem. C* **2013**, *1*, 7400−7408.
(11) Yamaguchi, Y.; Ogawa, K.; Nakayama, K.-I.; Ohba, Y.; Katagiri, H. *J. Am. Chem. Soc.* **2013**, *135*, 19095−19098.
(12) Wang, F.; Lai, Y.-H.; Kocherginsky, N. M.; Kosteski, Y. Y. *Org. Lett.* **2003**, *5*, 995−998.
(13) Lacroix, P. G.; Malfant, I.; Iftime, G.; Razus, A. C.; Nakatani, K.; Delaire, J. A. *Chem.—Eur. J.* **2000**, *6*, 2599−2608.
(14) Cristian, L.; Sasaki, I.; Lacroix, P. G.; Donnadieu, B.; Asselberghs, I.; Clays, K.; Razus, A. C. *Chem. Mater.* **2004**, *16*, 3543−3551.
(15) Salman, H.; Abraham, Y.; Tal, S.; Meltzman, S.; Kapon, M.; Tessler, N.; Speiser, S.; Eichen, Y. *Eur. J. Org. Chem.* **2005**, 2207−2212.
(16) Zieliński, T.; Kędziorek, M.; Jurczak, J. *Chem.—Eur. J.* **2008**, *14*, 838−846.
(17) Churchill, M. R. *Prog. Inorg. Chem.* **1970**, 53−98.
(18) Wada, E.; Nakai, T.; Okawara, M. *J. Polym. Sci., Polym. Chem. Ed.* **1978**, *16*, 2085−2087.
(19) Kurita, Y.; Kubo, M. *J. Am. Chem. Soc.* **1957**, *79*, 5460−5463.
(20) *Organic Photochemistry and Photophysics*; Ramamurthy, V., Schanze, K. S., Eds.; CRC Press: Boca Raton, FL, 2006.
(21) Pariser, R. *J. Chem. Phys.* **1956**, *25*, 1112−1116.
(22) Pariser, R. *J. Chem. Phys.* **1956**, *24*, 250−268.

(23) Diau, E. W. G.; De Feyter, S.; Zewail, A. H. *J. Chem. Phys.* **1999**, *110*, 9785−9788.
(24) Yamaguchi, H.; Sato, S.; Yasunam, M.; Sato, T.; Yoshinobu, M. *Spectrochim. Acta, Part A* **1997**, *53*, 2471−2473.
(25) Kasha, M. *Faraday Discuss.* **1950**, *9*, 14−19.
(26) Viswanath, G.; Kasha, M. *J. Chem. Phys.* **1956**, *24*, 574−577.
(27) Beer, M.; Longuet-Higgins, H. C. *J. Chem. Phys.* **1955**, *23*, 1390−1391.
(28) Danyluk, S. S.; Schneider, W. G. *J. Am. Chem. Soc.* **1960**, *82*, 997−998.
(29) Frey, H. M. *J. Chem. Phys.* **1956**, *25*, 600−601.
(30) Dunsch, L.; Rapta, P.; Schulte, N.; Schlüter, A. D. *Angew. Chem., Int. Ed.* **2002**, *41*, 2082−2086.
(31) Early, K. T.; Sudeep, P. K.; Emrick, T.; Barnes, M. D. *Nano Lett.* **2010**, *10*, 1754−1758.
(32) Yalcin, S. E.; Yang, B. Q.; Labastide, J. A.; Barnes, M. D. *J. Phys. Chem. C* **2012**, *116*, 15847−15853.
(33) Boudevska, H.; Brutchkov, C.; Astroug, H. *Eur. Polym. J.* **1983**, *19*, 737−741.
(34) Holden, D. A.; Guillet, J. E. *Macromolecules* **1980**, *13*, 289−295.
(35) He, Z.; Wu, H.; Cao, Y. *Adv. Mater.* **2014**, *26*, 1006−1024.
(36) Liu, F.; Page, Z. A.; Duzhko, V. V.; Russell, T. P.; Emrick, T. *Adv. Mater.* **2013**, *25*, 6868−6873.
(37) Page, Z. A.; Liu, F.; Russell, T. P.; Emrick, T. *Chem. Sci.* **2014**, *5*, 2368−2373.